Interception efficiency in two-dimensional flow past confined porous cylinders

Setareh Shahsavari*, Brian L. Wardle†, Gareth H. McKinley*[1]

**Department of Mechanical Engineering, †Department of Aeronautics and Astronautics, Massachusetts Institute of Technology, Cambridge, Massachusetts 02139, United States of America*

Abstract

The flow interception efficiency, which provides a measure of the fraction of streamlines that intercept a porous collector, is an important parameter in applications such as particle capture, filtration, and sedimentation. In this work, flow permeation through a porous circular cylinder located symmetrically between two impermeable parallel plates is investigated numerically under different flow and geometrical conditions. A flow interception efficiency is defined and calculated based on the flow permeation rate for a wide range of system parameters. The dependencies on all physical variables can be captured in three dimensionless numbers: the Reynolds number, the Darcy number (ratio of permeability to the square of cylinder diameter), and the plate separation relative to the cylinder size. The flow interception efficiency is very low in the limit of unbounded cylinders but significantly increases by restricting the flow domain. The fluid permeation rate through the porous cylinder varies nonlinearly with the relative plate/cylinder spacing ratio, especially when the gap between the cylinder and the confining plates is small compared to the cylinder size. In general, the effects of the Reynolds number, the Darcy number, and confinement on the flow interception efficiency are coupled; however, for most practical cases it is possible to factorize these effects. For practical ranges of the Darcy number ($Da < 10^{-4}$, which means that the pore size is at least one order of magnitude smaller than the porous cylinder diameter), the interception efficiency varies linearly with Da, is independent of the Reynolds number at low Reynolds numbers ($Re_D < 10$), and varies linearly with Reynolds number at higher flow rates. In addition to numerical solutions, theoretical expressions are developed for the flow interception efficiency in two limiting cases of confined and unbounded flow, based on modeling the system as a network of hydrodynamic resistances, which agree well with the numerical results. Furthermore, an expression for

[1] Corresponding author; email: gareth@mit.edu

the drag coefficient on the porous cylinder is proposed as a function of the Darcy number which can be used in the limit of large plate/cylinder relative spacing.

Nomenclature

C_D	[-]	drag coefficient	R	[Pa.s.m^{-2}]	pressure resistance
d_p	[m]	pore size	Re_D	[-]	Reynolds number $= \rho UD/\mu$
D	[m]	cylinder diameter	Re_H	[-]	Reynolds number $= \rho UH/\mu$
Da	[-]	Darcy number	Re_p	[-]	Reynolds number $= \rho U_a d_p/\mu$
H	[m]	plate separation	s	[m]	fiber spacing in fibrous media
L_r	[-]	ratio of plates separation to cylinder diameter (H/D)	S^*	[-]	dimensionless position of plate in polar coordinate
n	[-]	unit normal vector of surface	**u**	[ms^{-1}]	velocity vector
p	[Pa]	Pressure	u_θ	[ms^{-1}]	tangential velocity component
Q	[m^{2}s^{-1}]	volumetric flow rate per unit depth	U	[ms^{-1}]	mean velocity in free region
r	[m]	radius in polar coordinates	U_a	[ms^{-1}]	apparent velocity
r^*	[-]	dimensionless radius			

Greek symbols

δ	[-]	perturbation parameter	κ	[m^2]	permeability
ε	[-]	porosity	μ	[kgm^{-1}s^{-1}]	fluid dynamic viscosity
η	[-]	interception efficiency	Π	[-]	dimensionless pressure gradient
θ	[rad]	angle in polar coordinates	ρ	[kgm^{-3}]	fluid density

1. Introduction

Viscous flow past porous bodies is of importance in various fields of science and technology including many applications of chemical engineering (Neale et al., 1973; Sutherland and Tan, 1970), specifically in porous reactors (Drott et al., 1999), filtration, and sedimentation (Liu and Wang, 1997; Vanni, 2000), as well as in biomedical research where microfluidic systems are being developed for cell separation (Chen et al., 2012) or DNA purification (Chen et al., 2007). In such applications, fluid from a microchannel must permeate into a porous collecting element which is designed to serve as a highly sensitive detector for biomarkers. The primary benefit of using a porous medium is enhancement of the physical interaction between a solid surface (coated with biomarker receptors) and a test liquid (such as blood or sputum samples) by providing a higher surface area to volume ratio as well as by mitigating the effects of the mass transfer boundary layer that forms adjacent to a solid impermeable body and inhibits suspended particles from approaching the surface.

The porous collector typically consists of either a solid with interconnected pores or an aggregate of particles or fibers. When the fluid domain only involves a porous medium, the fluid motion through the medium can be described by Darcy's law. However, when an interface between a porous region and a free flow zone exist, the interaction between the restricted and unrestricted flow domains needs to be considered. One analytical technique that is used in the literature to account for this interaction is through application of matched asymptotic expansions that couple the inner Darcy flow and outer Stokes flow (Shi and Braden Jr, 1966; Singh and Gupta, 1971). Such methods are typically valid only at low Reynolds numbers (creeping flow regime). To study flow over a wider range of Reynolds number, numerical techniques are preferable. Here, we use a numerical model to study the inner and outer flow past a porous cylinder over a wide range of channel Reynolds numbers and Darcy numbers (dimensionless permeability) with a focus on calculation of the flow interception efficiency.

Flow interception efficiency is the fraction of flow streamlines that are intercepted by a porous collector compared to the streamlines that intercept the same projected area in an unrestricted flow. This is a key parameter in filtration and particle isolation applications

(Tufenkji and Elimelech, 2004), where the particles are isolated from a fluid as a result of direct interception, diffusion, inertial impaction, gravitational sedimentation, or chemical reaction (e.g. in chemically functionalized porous collectors).

The flow interception efficiency defined in this study is also equivalent to the permeation velocity factor, which is the ratio of the apparent (or superficial) velocity in the porous region to the free stream velocity (Sutherland and Tan, 1970). The significance of the permeation velocity arises from analyses of transport phenomena in porous media. It can be used to estimate the rate of transport by convection or for calculation of reactant residence time for reactions in permeable catalysts or in any system involving the interface of a porous material and a free stream.

The objective of this work is to investigate the effects of various physical parameters such as the permeability of the porous medium, fluid viscosity, flow rate, and channel dimensions on the flow permeation rate in the two-dimensional steady state laminar flow of Newtonian fluids past a porous cylinder of diameter D, porosity ε, and permeability κ, which is confined symmetrically between parallel plates that are separated by a distance H.

A theoretical analysis of flow past a permeable cylinder was first presented by Shi and Braden (Shi and Braden Jr, 1966) using a matched asymptotic expansion method to study creeping flow past an unbounded porous circular cylinder. They solved for the stream function and presented an analytical expression for the drag coefficient as a function of a dimensionless permeability. Singh and Gupta (Singh and Gupta, 1971) used a similar approach to obtain the solution for low Reynolds number flow past a cylinder with different permeabilities in the core region and in the outer shell. Bhattacharyya et al. (Bhattacharyya et al., 2006) used a finite volume method to numerically investigate the influence of permeability on the drag coefficient and streamlines and vorticity pattern in flow past an unbounded permeable cylinder. In their study the Reynolds number (based on the cylinder diameter) was varied between 1 and 40. Taking a similar approach, Yu et al. (Yu et al., 2011) numerically studied the steady viscous flow over (and through) a porous circular cylinder. They investigated the effects of fluid inertia (for $Re < 40$) and permeability ratio, on the flow pattern and occurrence

of a recirculating wake and calculated the critical Reynolds number for onset of a recirculating wake as a function of Darcy number, Da, which is defined as the ratio of the cylinder permeability to the square of the cylinder diameter.

All of the previous studies have considered an unbounded domain for the flow. However, in practical applications such as microfluidic devices, the porous collecting elements are influenced by the presence of adjacent impermeable surfaces such as bounding walls which can significantly affect the flow pattern. Therefore, in this study we consider the case of a porous circular cylinder in a confined flow.

Moreover, the main focus of previous studies have been on flow patterns and the overall drag coefficient. Here we focus on the flow interception efficiency and investigate the different factors that affect interception efficiency in the flow regime of a typical microfluidic system. A representative example of the application is the device developed by Fachin (Fachin et al., 2011) which integrated nanoporous elements composed of vertically aligned carbon nanotubes in a microfluidic systems, and illustrated their use in simultaneous chemical and mechanical isolation of bioparticles. The system described in that work consisted of a microchannel with dimensions $100\mu m \times 2mm$ containing cylindrical nanoporous elements of $200\mu m$ diameter with a Darcy number of 4×10^{-7}, and a characteristic channel Reynolds number of less than 10 (Fachin et al., 2011).

We introduce this prototypical microfluidic geometry as a canonical example for the range of the dimensionless numbers considered in present calculations. However, since we are employing a continuum approach, the results calculated for the drag coefficient and the interception efficiency as a function of the dimensionless system parameters (the Darcy number, the Reynolds number, and the plate separation ratio) can also be used for any other macroscale porous media flows that are also spanned by the range of physical parameters we explore.

2. Problem formulation

The problem domain is shown schematically in Figure 1 and the concept of the interception efficiency is shown in Figure 2. Here, we define the interception efficiency,

η, as the ratio of the flow rate passing through the cylinder to the flow rate through an infinitely permeable cylinder in an unbounded flow of uniform velocity U:

$$\eta = \frac{Q_c}{UD} \tag{1}$$

where Q_c denotes the two-dimensional volumetric flow rate (volumetric flow rate per unit depth) through the cylinder, U is the mean velocity between parallel plates, and D is the cylinder diameter. The interception efficiency defined in equation (1), is also equivalent to the ratio of the apparent velocity in the porous collector to the channel bulk velocity, U_a/U, which is sometimes called the permeation velocity factor.

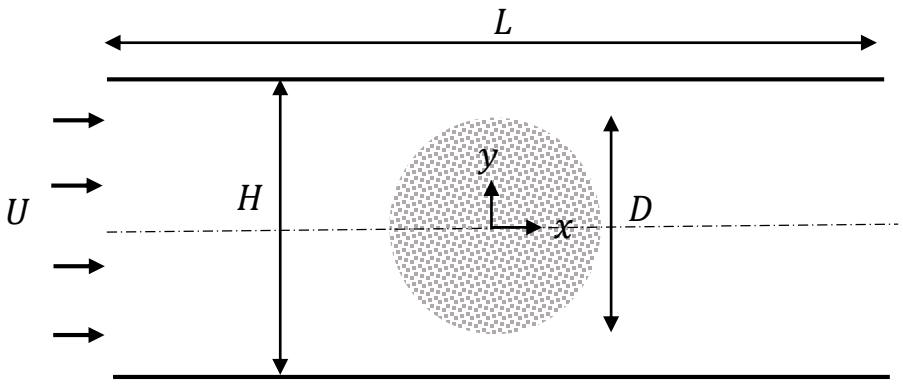

Figure 1: Schematic of a porous cylinder symmetrically placed between parallel impermeable plates

The parameters that affect the interception efficiency in a system consisting of flow past a single porous cylinder or an array of porous bodies with effective diameter D include the Reynolds number based on the scale of the object $Re_D = \rho UD/\mu$, the Darcy number $Da = \kappa/D^2$, and the relative distance of the porous body from other porous elements (for an array of porous collectors) or from a bounding wall (in case of a single porous cylinder). To investigate the effect of these parameters and analyze the flow characteristics for the system shown in Figure 1, we first develop a suitable numerical model. Then, we show that for two limiting cases, when the plates are close to the cylinder and when they are widely separated from each other, we can obtain simple analytical expressions for the interception efficiency as a function of the dimensionless system parameters.

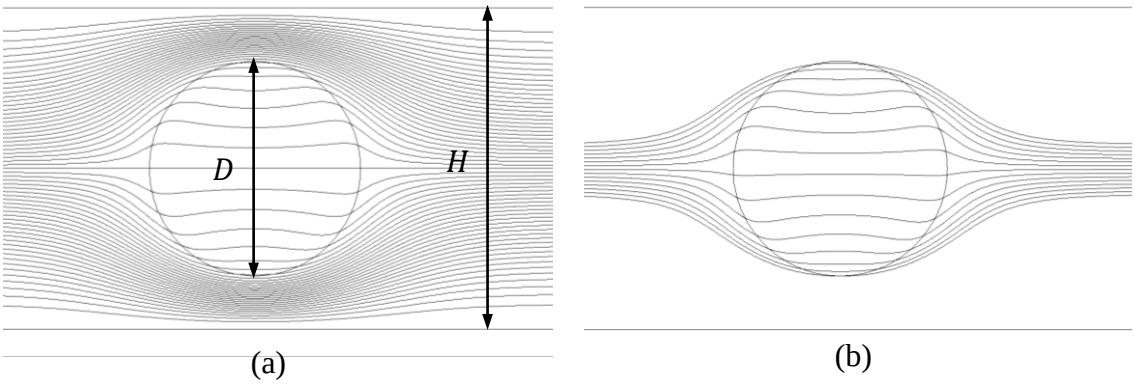

Figure 2: Concept of interception efficiency $\eta = Q_c/(UD)$ shown with streamlines in flow past a porous cylinder between parallel plates (a) evenly spaced streamlines representing the total flow rate $Q_{\text{tot}} = UH$ (b) isolating just the streamlines that intercept the cylinder, representing $Q_c = U_a D$

The governing equations in this problem are the Navier-Stokes equations for steady viscous flow in the channel, and the extended Darcy-Brinkman equation for the flow in the porous cylinder. In addition, mass should be conserved in the entire domain. For incompressible, steady state flow, we have the following set of equations, which respectively represent continuity, the momentum equation in the free region, and the momentum equation in the porous region i.e. the extended Darcy-Brinkman equation for homogeneous and isotropic porous materials.

$$\nabla . \mathbf{u} = 0 \tag{2}$$

$$\rho(\mathbf{u}.\nabla)\mathbf{u} = -\nabla p + \mu\nabla^2\mathbf{u} \tag{3}$$

$$\frac{\rho}{\varepsilon^2}(\mathbf{u}.\nabla)\mathbf{u} = -\nabla p + \frac{\mu}{\varepsilon}\nabla^2\mathbf{u} - \frac{\mu}{\kappa}\mathbf{u} \tag{4}$$

Here, $\mathbf{u}$ denotes the velocity vector, p is the pressure, ε and κ are the porosity and permeability of the porous material and ρ and μ denote the fluid density and viscosity. The momentum equation for the porous region, equation (4), includes both the inertial term and the viscous term. This equation reduces to the Brinkman equation when fluid inertia is negligible, i.e., when the Reynolds number based on the pore size and pore scale velocity is smaller than unity.

At the interface of the free and porous regions, the pressure and velocity fields are continuous. The boundary conditions we consider are i) uniform velocity at the inlet

($x = -L/2$); $\mathbf{u} = -U\mathbf{n}$, where $\mathbf{n}$ is the unit normal to the surface defining the outer boundary of the domain, ii) zero relative pressure and no viscous traction at the outlet ($x = L/2$); $p = 0$, and $\mu(\nabla\mathbf{u} + (\nabla\mathbf{u})^T).\mathbf{n} = 0$, and iii) no slip on the rigid bounding plates ($y = \pm H/2$); $\mathbf{u} = 0$. The axes and parametric channel dimensions are shown in Figure 1.

The set of equations (2)-(4) are numerically solved by the finite element method using COMSOL Multiphysics 4.3a, for a wide range of Reynolds number $Re_D = \rho UD/\mu$, plate separation ratio, $L_r = H/D$, and Darcy number, defined as $Da = \kappa/D^2$.

Depending on the relative separation between the plates, differing numbers of grid elements ranging from $N_{\text{grid}} = 10^4$ to $N_{\text{grid}} = 5 \times 10^5$ were used to achieve grid-independent and converged results.

3. Flow patterns

For steady viscous flow past a bounded porous cylinder, the flow pattern is governed by the dimensionless parameters Da, Re, and L_r. Regarding the effect of Reynolds number, we first note that in this problem, three independent length scales (H, D, and average pore size, d_p), and two velocity scales (the channel velocity, U, and apparent or superficial velocity in the porous cylinder, U_a) exist. Accordingly three Reynolds numbers can be defined: $Re_H = \rho UH/\mu$, $Re_D = \rho UD/\mu$, and $Re_p = \rho U_a d_p/\mu$, all of which affect the dynamics of the flow. Alternatively, one can specify one Reynolds number and two dimensionless geometric ratios. In order to specify the significance of inertial effects in the free region, the channel Reynolds number Re_H should be evaluated, while to predict the onset of vortex shedding, the cylinder Reynolds number Re_D is the key parameter. Finally, to decide whether the Forchheimer term, which accounts for the inertial effects in porous media (Vafai, 1984; Whitaker, 1996), needs to be accounted for the momentum equation it is necessary to determine the pore-based Reynolds number, Re_p.

In this study we focus on the regime where the Reynolds number based on the pore size is small ($Re_p \ll 1$, which is usually the case for real applications) and consequently, inertial effects inside the porous region can be neglected. We choose to report our results

in terms of the cylinder Reynolds number R_D and the channel spacing ratio $L_r = H/D$. In our parametric studies, the channel Reynolds number, Re_H, typically varies from 10^{-2} to 10^3.

We can use symmetry at the channel centerline to reduce the size of the computational domain for Reynolds numbers $Re_D < 40$. This symmetry breaks due to transition from steady flow to periodic vortex shedding regime at $Re_D > 40$ for an unbounded cylinder ($L_r \to \infty$) and at higher Reynolds numbers for bounded cylinders. The presence of a rigid wall near the cylinder delays the onset of vortex shedding and increases the critical Reynolds number. This has been well studied for solid circular cylinders placed between parallel plates (Chen et al., 1995; Sahin and Owens, 2004; Singha and Sinhamahapatra, 2010; Zovatto and Pedrizzetti, 2001). Chen et al. (Chen et al., 1995) numerically showed that the critical Reynolds number for separation of the flow over an impermeable cylinder located at the center of a channel is increased from $Re_D = 50$ to 90 as the blockage ratio is increased from 0.1 to 0.7 (or equivalently as L_r is decreased from 10 to 1.4).

The effect of permeability on the flow transition from steady to periodic viscous flow was studied for the case of an unbounded solid circular cylinder wrapped in a porous layer by Bhattacharyya and Singh (Bhattacharyya and Singh, 2011) and also for the case of an unbounded porous square cylinder by Babu and Narasimhan (Babu and Narasimhan, 2010) and by Jue (Jue, 2004). These studies show that high permeability ($Da > 10^{-4}$) dampens the vortex shedding behind the cylinder. For more practical Darcy numbers $Da < 10^{-4}$, we find from our transient numerical solution that the stability behavior and the shape of the streamlines outside the porous cylinder is similar to that of a solid cylinder.

We have also investigated the effect of confinement on the streamlines inside the porous cylinder. Figure 3 shows the effect of the presence of a rigid bounding wall on the shape of streamlines and pressure contours inside and outside of a porous cylinder. At low Reynolds numbers, based on an analysis of the shape of the streamlines, we can distinguish two limiting flow patterns inside the porous region that are controlled by the relative plate separation: i) when the plates are close to the cylinder, the streamlines

inside the porous cylinder are initially orthogonal to the cylinder boundary as shown in Figure 3 (a), ii) conversely, when the plates are far away from the cylinder ($L_r \gg 1$), as is the case in Figure 3 (c), the streamlines are straight lines parallel to the main flow stream and concomitantly the pressure contours are orthogonal to the flow direction. The characteristic scale for nondimensionalizing the pressure distribution is $\Delta p_c = \frac{\mu U_a}{D}\frac{1}{Da}$, which gives a pressure variation in the range of zero to $O(1)$. Rearranging this pressure scale, we obtain $\Delta p_c = \frac{\mu U}{D}\frac{\eta}{Da}$. The first part, $\frac{\mu U}{D}$, is the characteristic scale for the pressure drop due to viscous flow in the absence of bounding walls. The second part, η/Da, is an additional factor which captures the effect of geometry (i.e. the cylinder permeability and the plate separation ratio) on the magnitude of typical pressure variations.

This is the pattern for Darcy numbers $Da < 10^{-4}$ (corresponding to a porous cylinder with an average pore size that is at least one order of magnitude smaller than the cylinder diameter). For extremely high permeabilities ($Da > 10^{-2}$), streamlines inside the porous region are always parallel to the main flow direction regardless of the blockage ratio. In such cases, the pore size is in fact of the same order of magnitude as the cylinder size and thus the pores offer little viscous flow resistance. Table 1 gives typical Darcy numbers for fibrous materials at various porosities and relative fiber spacing based on the permeability equation developed by Tamayol and Bahrami (Tamayol and Bahrami, 2011). Even for a porosity of $\varepsilon = 0.9$ and a fiber spacing as high as $s/D = 0.1$, the Darcy number is in the order of 10^{-4}.

Table 1. Typical values of the Darcy number, $Da = \kappa/D^2$, for fibrous materials with different porosities and fiber spacing relative to the porous cylinder diameter, s/D. Permeability is calculated based on the expression developed by Tamayol and Bahrami (Tamayol and Bahrami, 2011) assuming periodic square arrangement of fibers.

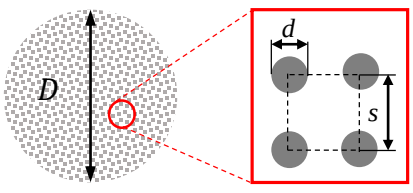

porosity, ε	$s/D = 0.0001$	0.001	0.01	0.1
0.5	2×10^{-11}	2×10^{-9}	2×10^{-7}	2×10^{-5}
0.7	1×10^{-10}	1×10^{-8}	1×10^{-6}	1×10^{-4}
0.9	4×10^{-10}	4×10^{-8}	4×10^{-6}	4×10^{-4}

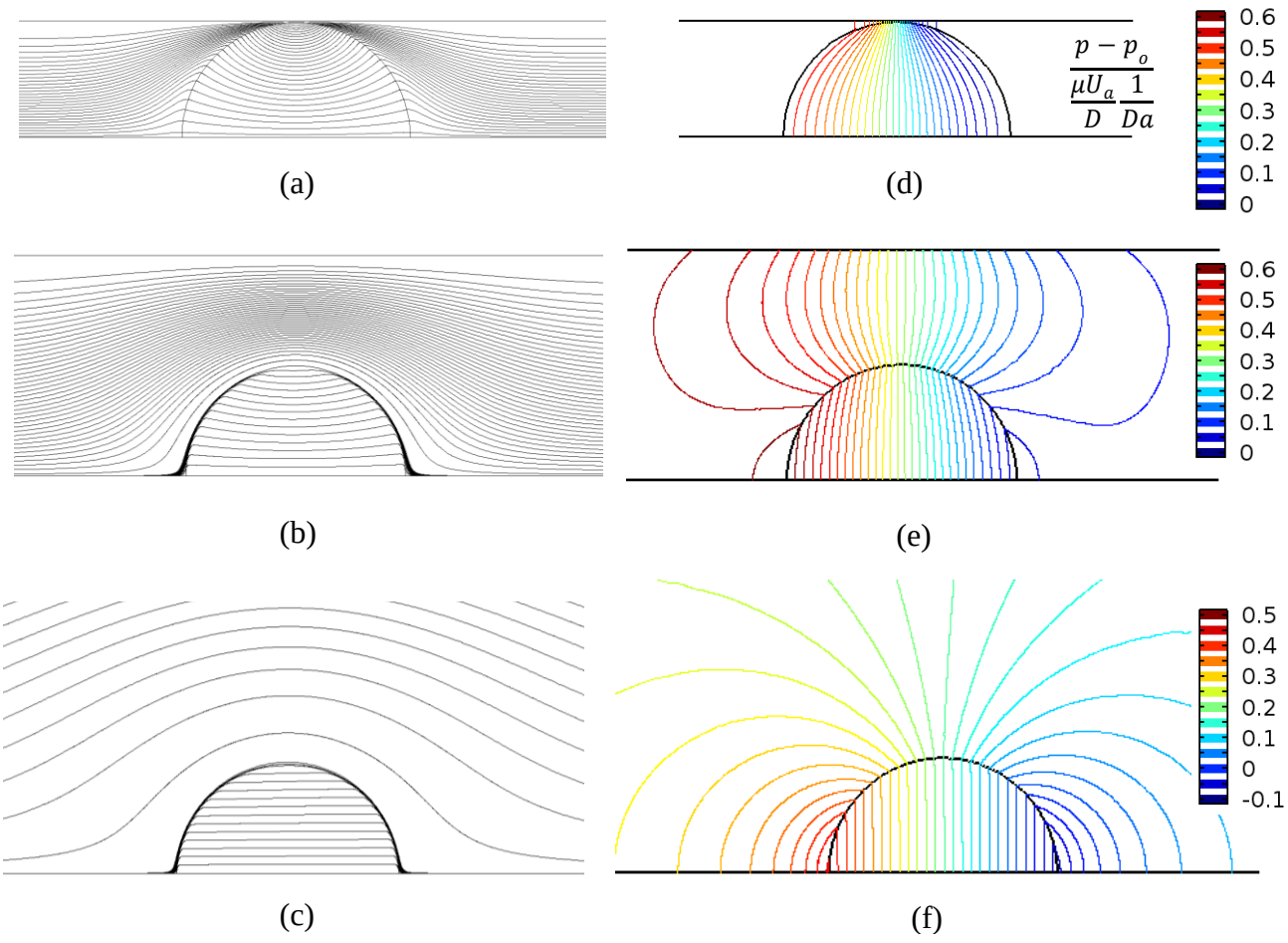

Figure 3: Effect of the relative location of the bounding walls on flow streamlines and contours of the dimensionless pressure $(p-p_o)/(\frac{\mu U_a}{D}\frac{1}{Da})$ inside and outside a confined porous cylinder: (a) streamlines $L_r = 1.01$, (b) streamlines L_r =2, (c) streamlines $L_r = 20$, (d) pressure $L_r = 1.01$, (e) pressure $L_r = 2$, (f) pressure L_r =20. For all cases $Re_H = \rho UH/\mu = 0.5$ and $Da = 10^{-5}$. In figure (a) streamlines inside and outside the cylinder are evenly spaced based on their magnitude, while in figures (b) and (c) due to the very low interception efficiency, streamlines inside the porous cylinder are controlled by specifying starting point coordinates at $x = -L/2$ from $y = 0$ to $y = DU_a/U$.

4. Parametric studies

Parametric studies were conducted to investigate the effect of changing the cylinder permeability, viscous fluid properties, flow rate, and system dimensions on the computed interception efficiency. Changes in these parameters can be fully captured in

three dimensionless groups: the Darcy number, the channel Reynolds number, and the relative separation of the plates, $L_r = H/D$. Figure 4 shows the results for the interception efficiency as the Darcy number is varied. In all the plots, the interception efficiency is calculated using equation (1) based on Q_c, which can be obtained by integrating the horizontal velocity profile, u_x, at $x = 0$ from $y = -D/2$ to $D/2$. Figure 4 shows that for Darcy numbers $Da < 10^{-4}$, the interception efficiency increases linearly with the permeability of the porous material at the studied Reynolds numbers. At high Darcy numbers all of the curves asymptote towards a limiting efficiency of unity.

The effect of the relative distance between the cylinder and the bounding plates, L_r, is presented in Figure 5. For $L_r < 3$, the variation of interception efficiency with L_r is highly nonlinear. As the blockage ratio decreases ($L_r \gg 1$), the effect of the plates on the flow through the porous cylinder becomes negligible.

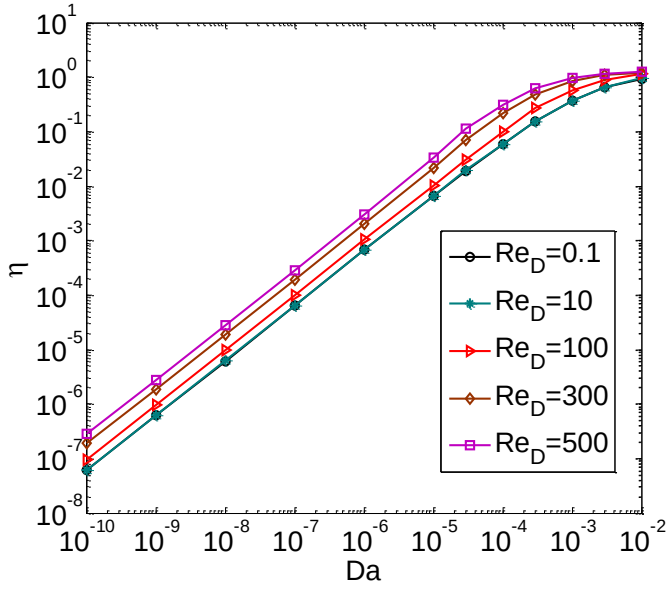

Figure 4: Interception efficiency with variation of the Darcy number at different Reynolds numbers for plate separation ratio of $L_r = 1.5$. The lines are drawn to connect the numerical data points.

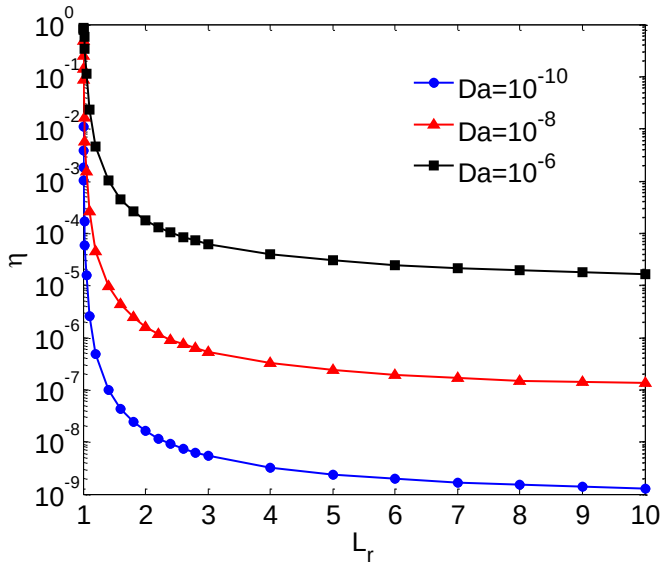

Figure 5: The effect of varying the channel spacing ratio, L_r, on the interception efficiency at different Darcy numbers, for a fixed Reynolds number $Re_D = 1$.

The effect of fluid inertia on the interception efficiency is presented in Figure 6. To rationalize the trends observed in Figure 6, we need to consider the scale of the pressure gradient that is driving the flow through the cylinder. The pressure drop due to motion of a fluid in any system with viscous friction and inertia has a quadratic relation with the fluid velocity, which was first formulated by Osborne Reynolds as noted by Ergun (Ergun, 1952). Therefore, the pressure drop induced by viscous flow past the cylinder in the channel can be written in the form:

$$\frac{\Delta p}{D} = a\mu U + b\rho U^2 \qquad (5)$$

where the constants a and b are functions of the system geometry and U is the mean velocity in the channel. Similarly, we can write an analogous relation for the pressure drop through the porous cylinder by replacing the channel mean velocity, U, by the characteristic velocity in the porous region, U_a, only with different coefficients. At the interface of the two regions, the pressure must be the same on both sides of the interface and we can equate the pressure scale from the free and porous regions. For low Darcy

numbers ($Da < 10^{-3}$) we expect $U \gg U_a$ or $Re_D \gg Re_p$. The term including U_a^2 is thus negligible compared to the other terms, as a result we have

$$a'\mu U_a = a\mu U + b\rho U^2 \tag{6}$$

Rearranging this we have

$$\frac{U_a}{U} = (1 + cRe_D)f \tag{7}$$

The proportionality factor f is a function of the Darcy number and the relative separation distance of plates. Equation (7) in fact, presents the trend we see in Figure 6, where the interception efficiency η, or equivalently, the permeation velocity factor U_a/U, transitions gradually from an initially constant value at low flow rates, and at high Reynolds numbers ($Re_D > 100$) increases linearly with Re_D. Regressions of the numerical results to equation (7) at high Reynolds numbers renders the constant $c = 0.01$ for $L_r = 1.5$. In the following section, we will derive analytical expressions for the proportionality factor f based on approximate solutions for the pressure drop in the two limiting cases of compact channel spacing (i.e. $L_r \to 1$) and an unbounded porous cylinder ($L_r \to \infty$).

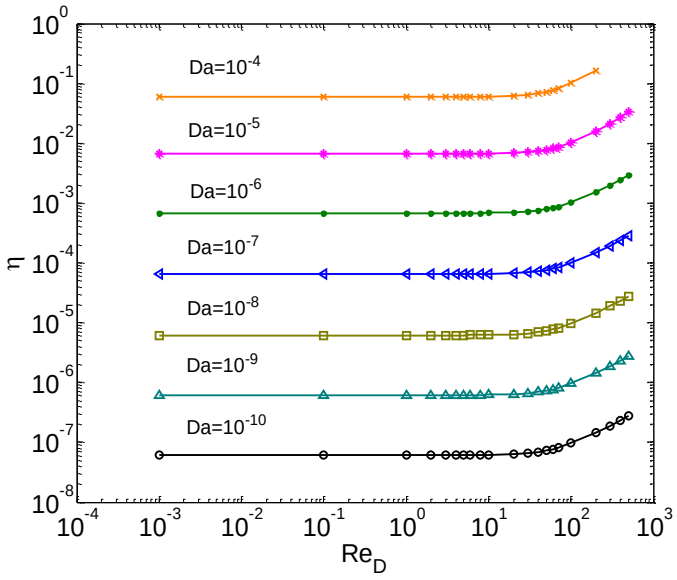

Figure 6: Interception efficiency varying with Reynolds number at different Darcy numbers, $L_r = 1.5$. The lines are drawn to connect the numerical data.

5. Analytical solution for $L_r \to 1$

To find an analytical expression for the interception efficiency in the limit that the gap between the cylinder and plates is small, we employ a resistance network model, in which the flow resistance is defined as the pressure drop along the path divided by the volumetric flow rate through the path. The equivalent circuit for a porous cylinder located between parallel plates is shown in Figure 7 (a). In this figure, R_g and R_c represent respectively, the flow resistance of the gap between each plate and the cylinder and the flow resistance of the porous cylinder. The volumetric flow rates per depth corresponding these resistances are Q_g and Q_c respectively.

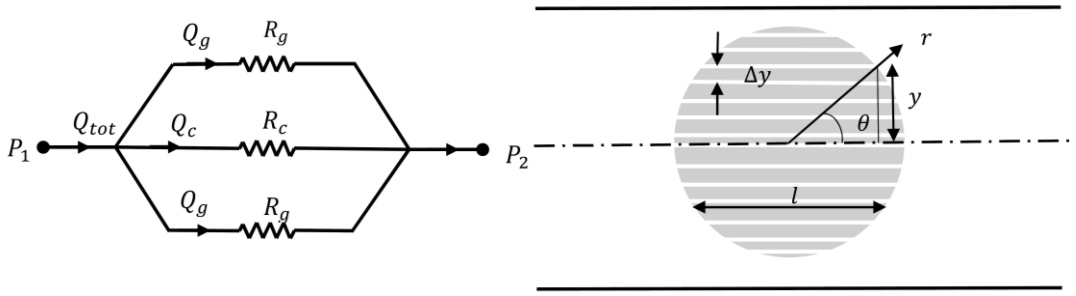

(a) (b)

Figure 7: (a) Equivalent resistance network model, (b) porous cylinder considered as parallel elements for resistance calculation.

Using this resistance model, the dimensionless flow rate through the porous cylinder is obtained as $\eta = (Q_c/Q_{tot})(H/D) = L_r Q_c/(Q_c + 2Q_g)$. The volumetric flow rates are inversely proportional to the hydrodynamic resistances, therefore,

$$\eta = \frac{Q_c}{UD} = \frac{L_r}{1 + \frac{2R_c}{R_g}}. \tag{8}$$

The porous cylinder resistance, R_c, can be considered as the equivalent resistance of a network of thin parallel elements as shown schematically in Figure 7 (b). The gap resistance, R_g, is found based on the velocity field around the cylinder and the local geometry. In the following sections we derive expressions for each of the pressure resistances R_c and R_g.

5.1. Porous cylinder resistance

By assuming that the streamlines inside the porous cylinder are parallel to the main flow stream, the resistance of the porous cylinder can be obtained by dividing it into a network of infinitesimally thin parallel elements as schematically shown in Figure 7 (b). Each element has resistance $R_{c,i}$ and the total resistance is $R_c = \left(\sum R_{c,i}^{-1}\right)^{-1}$. Using Darcy's law, the pressure drop through each element is

$$\Delta p = \left(\frac{\mu l}{\kappa \Delta y}\right) Q_i \tag{9}$$

where Q_i is the two-dimensional volumetric flow rate through each element. The coefficient in parentheses in front of Q_i on the right hand side of equation (9) is the element resistance $R_{c,i}$. As a result, we obtain the following equation for calculating the total resistance.

$$R_c = \left(\int_{-\frac{D}{2}}^{\frac{D}{2}} \frac{\kappa dy}{\mu l}\right)^{-1} \tag{10}$$

Substituting $l = D\cos\theta$ and $dy = (D/2)\cos\theta\, \mathrm{d}\theta$ in equation (10) and integrating from $\theta = -\pi/2$ to $\pi/2$, the equivalent resistance of a permeable cylinder can be calculated to be

$$R_c = \frac{2\mu}{\pi\kappa} \tag{11}$$

Note that the cylinder resistance, R_c, does not depend on cylinder diameter, D; however, for a constant velocity, as we expect the pressure drop varies linearly with D since the volumetric flow rate directly depends on D, when we set the velocity to be constant. In deriving equation (11), we did not make any assumption on L_r so this result can be used for bounded and unbounded porous cylinders.

5.2. Flow around the cylinder in the narrow gap limit

The flow resistance arising from steady viscous flow in the gap between the plate and the cylinder is obtained by solving a simplified momentum equation in cylindrical coordinates, assuming a no slip boundary condition on the porous cylinder. This assumption is justified only for use in the resistance model being considered here. In fact

in the limit of $L_r \to 1$, the tangential slip velocity at the surface of the cylinder can be relatively high; however, in this limit the gap resistance is much higher than the porous cylinder resistance ($R_g \gg R_c$), which leads to $\eta \to 1$ in equation (8) as expected. For larger values of L_r, as the relative distance between the porous object and the plates increases, the slip velocity becomes much smaller compared to the free region velocity. For instance at $L_r > 1.2$, according to our numerical simulations, the ratio of the average slip velocity along the cylinder perimeter compared to the average velocity in the gap is less than 5% for $Da < 10^{-5}$, and less than 1% for $Da < 10^{-6}$. To illustrate this we show in Figure 8 (on a semi-logarithmic scale) the dimensionless velocity field inside the cylinder ($y \le D/2$) and in the gap outside the cylinder ($D/2 \le y \le H/2$). From this figure, we see that for $Da < 10^{-4}$, the velocity at the interface of the porous cylinder (indicated by the hollow circle) is much smaller than the velocity in the gap. The assumption of no slip at the interface between the free stream and the porous cylinder is thus quite reasonable for most practical values of the permeability.

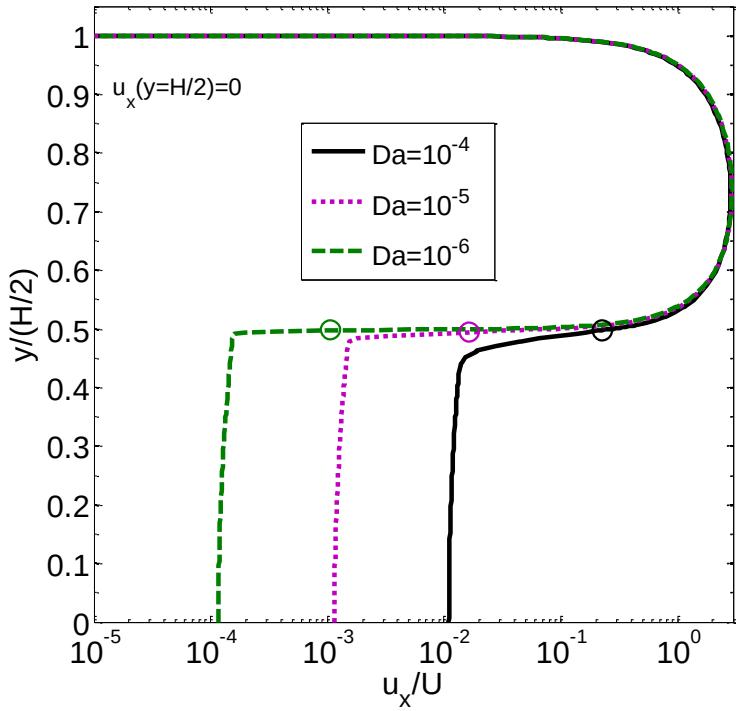

Figure 8. The velocity profile inside and outside the porous cylinder at $x = 0$ obtained from the numerical solution at different Darcy numbers for $L_r = H/D = 2$ and $Re_H = 0.1$. The hollow circle at $y/(H/2) = 0.5$ indicates the velocity at the interface of the porous cylinder and the side channel.

Consistent with the lubrication approximation approach, we assume that around the cylinder the flow is locally fully-developed. Taking cylindrical polar coordinates to describe the flow around the cylinder, we assume that in the narrow gap limit the principal velocity component is the tangential velocity, v_θ, the radial velocity is negligible, and the pressure only varies in tangential direction so that $\frac{\partial p}{\partial r} = 0$. Under these assumptions, the tangential component of the Navier-Stokes equations is reduced to

$$\mu\left(\frac{1}{r}\frac{\partial}{\partial r}\left(r\frac{\partial u_\theta}{\partial r}\right) - \frac{u_\theta}{r^2}\right) = \frac{1}{r}\frac{\partial p}{\partial \theta}. \tag{12}$$

Introducing dimensionless variables for the radial position, $r^* = \frac{r}{D/2}$, the pressure gradient, $\Pi = \frac{D}{2\mu U}\frac{\partial p}{\partial \theta}$, and velocity, $u^* = \frac{u_\theta}{U}$, yields a non-dimensional form of equation (12):

$$r^{*2}u^{*\prime\prime} + r^* u^{*\prime} - u^* = \Pi\, r^* \tag{13}$$

where a prime denotes a derivative with respect to r. Equation (13) is the nonhomogeneous Euler differential equation. The solution is given by a the summation of the homogeneous and particular solutions

$$u^* = \frac{\Pi}{2}\left(r^* \ln r^* + k_1 r^* + \frac{k_2}{r^*}\right) \tag{14}$$

where k_1 and k_2 are constants that need to be determined by the boundary conditions. We apply the no slip condition on the cylinder in the channel ($r^* = 1$) and on the bounding plate ($r^* = S^* = \frac{L_r}{\sin\theta}$).

$$\begin{aligned} r^* = 1 &: \quad u^* = 0 \\ r^* = S^* &: \quad u^* = 0 \end{aligned} \tag{15}$$

In reality, there is a non-zero slip velocity at the interface of the cylinder as shown in Figure 8; however, it is small compared to the bulk velocity in the gap. James and Davis (James and Davis, 2001) derived an expression for an average slip velocity as a function of porosity for highly porous fibrous media ($\varepsilon > 0.9$) by finding solutions for Stokes flow in a channel partially filled with an array of circular fibers. Their study shows that even for sparse arrays, the dimensionless slip velocity is small. Nevertheless, for mesoscale modeling of porous media, a porosity-dependent slip velocity such as that

derived by James and Davis should be considered as the boundary condition at $r^* = 1$. Here for simplicity, we neglect the slip velocity in our theoretical approach and later we will see that the solution derived under this assumption agrees well with our numerical results.

Applying the boundary conditions (equation (15)) yields:

$$u^* = \frac{\Pi}{2}\left(r^* \ln r^* + \frac{S^{*2} \ln S^*}{S^{*2} - 1}\left(\frac{1}{r^*} - r^*\right)\right) \tag{16}$$

Integrating equation (16) from $r^* = 1$ to $r^* = S^*$ renders the relation between the tangential pressure gradient and the volumetric flow rate per depth, Q_g, as given by equation (17):

$$\frac{\partial p}{\partial \theta} = \frac{32\mu Q_g}{D^2}\left(\frac{S^{*2} - 1}{S^{*4} - 2S^{*2}\,(\,2(\ln S^*)^2 + \,1) + \,1}\right) \tag{17}$$

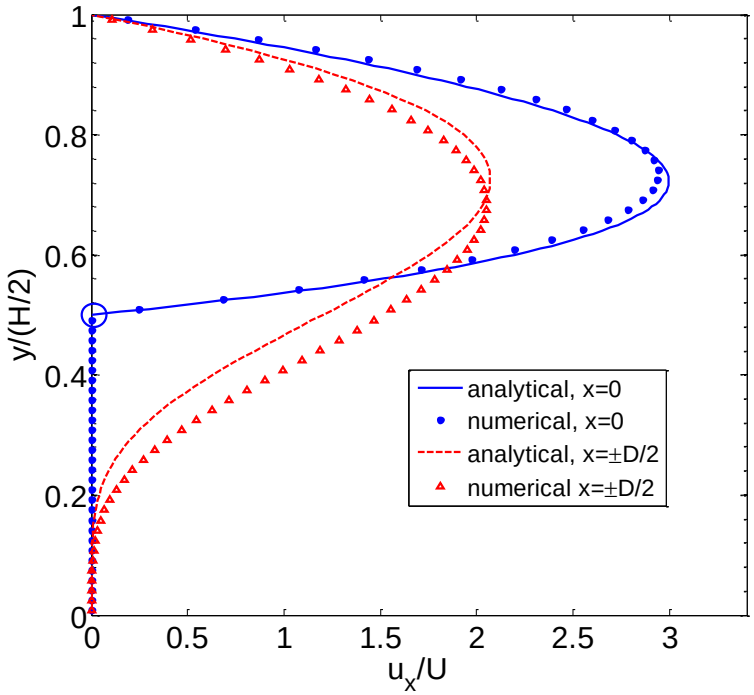

Figure 9: The x-component of the velocity in the gap at $x = 0$ and $x = \pm D/2$ from analytical solution (lines) for flow around solid cylinder and numerical solution (symbols) for flow past a porous cylinder with $Da < 10^{-4}$. In both cases, $Re_H = 0.5$, $L_r = 2$. The hollow circle at $y/(H/2) = 0.5$ indicates the velocity at the interface of the porous cylinder and the side channel at $x = 0$.

According to equations (16) and (17), at $\theta = 0$ and π, the tangential component of velocity vanishes. In fact at these points, velocity is solely in radial direction, which is in contradiction with our assumption of negligible radial velocity; however, since the tangential pressure gradient from equation (17) is zero at these points, it does not contribute to the total pressure drop that we obtain using this solution. Figure 9 compares the x-component of the velocity profile ($u_x = -u_\theta \sin\theta$) from analytical solution, equation (16), with numerical data at $x = 0$ and $x = \pm D/2$. At $x = 0$ we achieve the best agreement with numerical results since the radial velocity is zero at this line. The agreement becomes increasingly good as L_r is progressively decreased.

Substituting $S^* = \frac{L_r}{\sin\theta}$ into equation (17) and integrating from $\theta = 0$ to π, the total pressure drop for steady viscous flow past the cylinder is calculated as

$$\Delta p = \frac{32\mu\, I(L_r)}{D^2} Q_g \tag{18}$$

where $I(L_r)$ is a dimensionless function of L_r given by the following integral

$$I(L_r) = \int_0^\pi \frac{\sin^2\theta\,(\,L_r^2 - \sin^2\theta)}{(L_r^2 - \sin^2\theta)^2 - \left(2L_r \sin\theta \ln\frac{L_r}{\sin\theta}\right)^2} d\theta \tag{19}$$

The flow resistance of the gap between the cylinder and the wall is therefore,

$$R_g = \frac{32\mu\, I(L_r)}{D^2} \tag{20}$$

Equations (8), (11), and (20) can be combined to give an analytical expression for the interception efficiency in the Stokes flow limit as a function of Da and L_r:

$$f(L_r, Da) = \eta_{Re\to 0} = \frac{L_r}{1 + \left(2\pi\, Da\, I(L_r)\right)^{-1}} \tag{21}$$

Equation (21) provides a semi-analytic expression for the proportionality factor anticipated in eq. (7). This result is only suitable for low Reynolds numbers since inertial terms in the momentum equation were neglected. To include the effect of the Reynolds number, we combine equations (21) and (7) to obtain a more general expression for the interception efficiency in the narrow gap limit:

$$\eta = \frac{L_r(1 + cRe_D)}{1 + \left(2\pi\, Da\, I(L_r)\right)^{-1}} \tag{22}$$

Figure 10 shows that our numerical results for the interception efficiency (initially presented in Figure 6) can all be collapsed onto a single curve by combining the effects of the Darcy number and the relative separation of plates using equation (22). The inset plot in Figure 10 shows the function $I(L_r)$ calculated from numerical integration. It is instructive to inspect the behavior of η as $L_r \to 1$, since $I(L_r) \to \infty$ in this limit. Assuming $L_r = 1 + \delta$, where $0 < \delta \ll 1$, the Taylor expansion of $I(L_r)$ in equation (21), gives

$$\eta = \frac{1 + \delta}{1 + \frac{1}{3\pi\theta^* Da}\delta^3 + O(\delta^4)} \tag{23}$$

where θ^* is a coefficient between 0 and π which approaches zero as $L_r \to 1$. Therefore an upper bound for η in this limit is

$$\eta \leq \frac{1 + \delta}{1 + Da^{-1}\delta^3 + O(\delta^4)}. \tag{24}$$

Inspection of this upper bound suggests that the sufficient condition to achieve $\eta \to 1^-$, i.e., η approaches unity from below as $L_r \to 1^+$ is

$$\delta > \sqrt{Da} \tag{25}$$

which, if translated to dimensional form, means that the average pore size inside the cylinder should be smaller than the gap size between the porous cylinder and the side wall, otherwise L_r should be identically equal to unity.

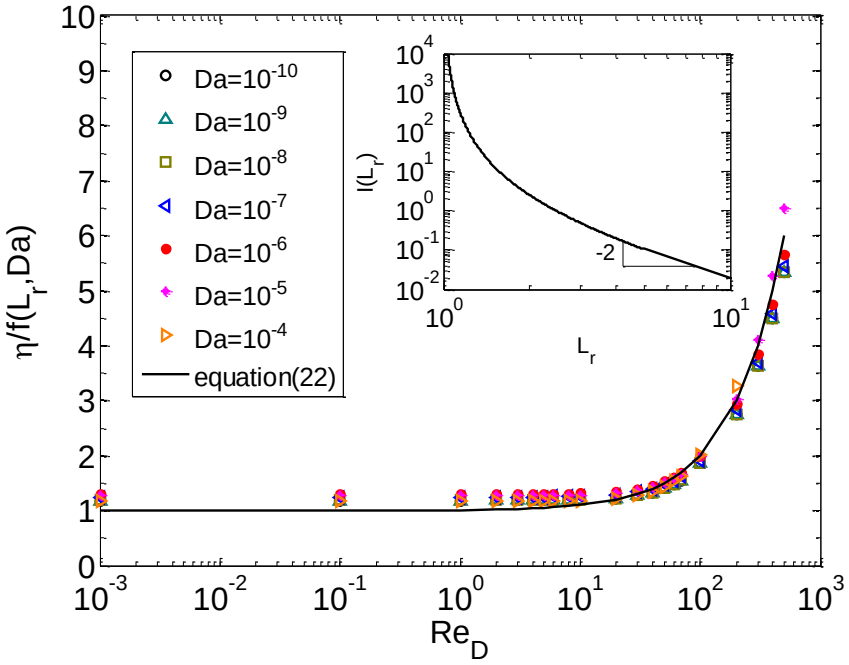

Figure 10: Interception efficiency varying with Reynolds number: the computed results shown in Figure 6 collapse by combining the effect of the Darcy number and the plate relative separation using $f(L_r, Da) = \eta_{Re\to 0}$ given in equation (21), the solid line is (22) with $c = 0.01$. The inset plot shows the function defined in equation (19), which is used to calculate $f(L_r, Da)$.

6. Theoretical limit for $L_r \to \infty$

In this section, we obtain an expression for the interception efficiency of porous cylinders in the limit of unbounded viscous flow. To find this limit we approximate the pressure drop resulting from the flow around and through a permeable cylinder with the drag force on the porous cylinder per projected area,

$$\Delta p \approx \frac{1}{2}\rho U_0^2 C_D \tag{26}$$

where C_D is the drag coefficient for flow past a porous cylinder and U_0 is the approach velocity at $y = 0$, far from the cylinder. The velocity U_0 is 1.5 times the channel mean velocity, U, for Poiseuille flow confined between parallel plates. Using this approximation for the pressure drop in combination with the cylinder resistance from equation (11), we calculate the flow rate through the cylinder, Q_c. Substituting Q_c into the definition of η given in equation (1), the following relation for the interception efficiency is obtained

$$\eta^* = \frac{Q_c}{U_0 D} = \frac{3\pi}{8}\, Re_D\, Da\, C_D \tag{27}$$

where η^* is the interception efficiency based on a slightly modified form of equation (1); specifically, we have used the centerline approach velocity, U_0, in the denominator instead of the channel mean velocity, U, in order to avoid efficiencies higher than 1 in the limit of $L_r = H/D \gg 1$.

An expression for the drag coefficient on a porous cylinder should satisfy two conditions: i) as $Da \to 0$, the drag coefficient converges to that of a solid cylinder and ii) as $Da \to \infty$, the drag coefficient should approach zero as the cylinder offers no resistance to the flow. For the case of a porous sphere, Sutherland and Tan (Sutherland and Tan, 1970) analytically derived the following equation for the low Reynolds number regime:

$$C_D^{\text{sphere}} = \frac{C_{D,0}^{\text{sphere}}}{1 + 6Da}. \tag{28}$$

where C_D^{sphere} is the drag coefficient of the porous sphere and $C_{D,0}^{\text{sphere}}$ denotes the drag coefficient of a solid sphere (with zero permeability) at the same Reynolds number. Based on the solution derived by Sutherland and Tan (Sutherland and Tan, 1970), the flow permeation factor for a porous sphere can be calculated to be

$$\eta^{\text{sphere}} = \frac{6Da}{1 + 6Da}. \tag{29}$$

Motivated by the expression for the drag coefficient derived by Sutherland and Tan (Sutherland and Tan, 1970), we assume the following form for the drag coefficient of a porous cylinder in an unbounded steady viscous flow:

$$C_D = \frac{C_{D,0}}{1 + \alpha\, Da} \tag{30}$$

where $C_{D,0}$ is the drag coefficient of the corresponding solid cylinder. The coefficient α is found by substituting equation (30) into equation (27) and considering the fact that η^* should converge to unity as $Da \to \infty$, which yields

$$\alpha = \frac{3\pi}{8}\, Re_D\, C_{D,0}. \tag{31}$$

Therefore, we propose the following relation for the drag coefficient of a permeable cylinder.

$$C_D = \frac{C_{D,0}}{1 + 3\pi/8\, Re_D\, C_{D,0}\, Da} \tag{32}$$

Expressions for the drag coefficient for flow past a solid circular cylinder are available in the literature for a wide range of Reynolds number (Happel and Brenner, 1983; White, 2011). For low Reynolds numbers (Stokes regime), Faxén (Faxén, 1946) has developed an analytical solution for flow past a solid cylinder between two parallel plates that symmetrically constrain the flow assuming that the plates spacing is much higher than the cylinder diameter. In Figure 11, the drag coefficient for a permeable cylinder is compared with the value for a solid cylinder at large values of $L_r = H/D$. The data for the permeable cylinder are based on our numerical simulations and the curve for the solid cylinder is based on Faxén's analytical solution (Faxén, 1946) using the first four terms in the series expansion, given as

$$C_{D,0} = \frac{8\pi}{Re(a_0 - \ln(L_r^{-1}) + a_2 L_r^{-2} + a_4 L_r^{-4} + a_6 L_r^{-6} + a_8 L_r^{-8})} \tag{33}$$

where, the coefficients are $a_0 = -0.915689$, $a_2 = 1.72438$, $a_4 = -1.730194$, $a_6 = 2.40564$, $a_8 = -4.59131$, and the Reynolds number is defined as $Re = \rho U_0 D/\mu$.

Figure 12 shows the effect of Darcy number on the drag coefficient of a permeable cylinder. In this figure, the results from numerical simulations at $L_r = 50$ are compared against equation (32) and the solution by Singh and Gupta (Singh and Gupta, 1971), which was obtained for creeping flow past unbounded cylinder and consequently does not depend on L_r. Since our numerical results for large values of L_r are in very good agreement with Faxén's solution, for calculating $C_{D,0}$ and its variation with L_r in equation (32) and (34), we use equation (33).

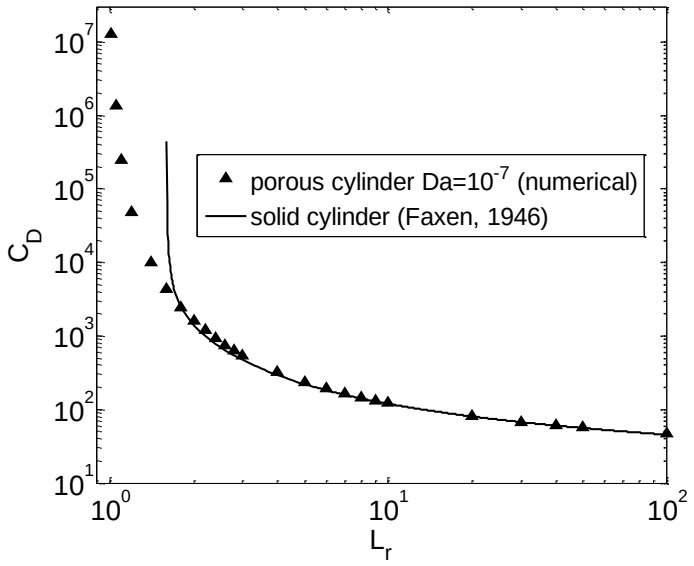

Figure 11: Variation in the drag coefficient of a porous cylinder with the plate separation ratio, $L_r = H/D$ at $Re_D = 0.1$. Numerical data (symbols) are for a porous cylinder at $Da = 10^{-7}$. The solid line is Faxén's solution for a solid cylinder using the first four terms in the series expansion.

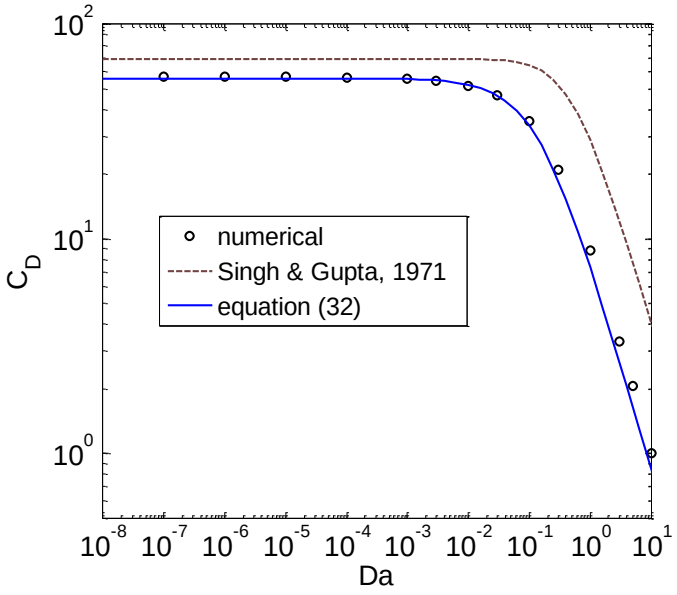

Figure 12: Drag coefficient on a porous cylinder varying with Darcy number at a fixed Reynolds number Re_D =0.1. Numerical results (symbols) are for $L_r = 50$, the analytical solution of Singh and Gupta (Singh

and Gupta, 1971) (dashed line) is independent of L_r, and $C_{D,0}$ in equation (32) (solid line) was calculated using Faxén's solution with the first four terms.

It is apparent from Figure 12 that under the condition of $L_r \gg 1$ and in the practical range of Darcy number ($Da < 10^{-4}$), the pressure drop resulting from flow past a porous cylinder is equal to that of a solid cylinder.

Combining equations (27) and (32), and considering that for flow between parallel plates $U_0 = \frac{3}{2}U$, the interception efficiency for viscous flow past an unbounded permeable cylinder η^* can thus be calculated from the following expression

$$\eta = \frac{3}{2}\eta^* = \frac{9\pi/16\ Da\ Re_D\ C_{D,0}}{1 + 3\pi/8\ Da\ Re_D\ C_{D,0}}. \qquad (34)$$

At low Reynolds numbers, the product of $Re_D\ C_{D,0}$ is constant for a fixed value of L_r (see equation (33)) and as $L_r \to \infty$, the interception efficiency merely depends on the dimensionless permeability. The results for η in this limit are similar to the permeation velocity factor for sedimentation of an unbounded porous sphere developed by Sutherland and Tan (Sutherland and Tan, 1970), given in equation (29).

7. Conclusions and Discussion

We have investigated steady viscous flow of a Newtonian fluid past and through a porous cylinder confined symmetrically between two rigid and impermeable parallel plates using a numerical approach. We have calculated the flow interception efficiency (which characterizes the percentage of the approaching flow in the channel that passes through the cylinder) for a wide range of system parameters. Furthermore, we have derived simple analytical expressions for this interception efficiency in two limiting cases of high and low blockage of flow around the cylinder. These expressions can be used as a basis for the analysis of heat and mass transport phenomena in porous cylindrical features or for calculating the capture efficiency in microfiltration processes such as the development of permeable sensing elements for collecting biomarkers in a microfluidic channel (Fachin et al., 2011).

Flow characteristics, such as the shape and magnitude of the streamlines inside the porous cylinder, are affected by the Darcy number, Reynolds number, and blockage

ratio. When there is a wide gap between the plates and cylinder ($L_r > 2$), the interception efficiency varies linearly with Da for all practical values of the Darcy number ($Da < 10^{-3}$). However, in the limit of $L_r \to 1$, the effect of the cylinder permeability on the interception efficiency is coupled to the relative separation distance of the bounding walls. The effect of fluid inertia on the interception efficiency is negligible at low Reynolds numbers and becomes more significant when $Re_D \gg 10$. This can be captured through a simple functional form such as equation (7) with $c = 0.01$ for $L_r > 1.1$.

The results from Sections 5 and 6 can be combined to show how the interception efficiency varies over the entire range of plate/cylinder relative spacing. Motivated by Figure 4 and by equations (22) and (34) we plot our results in terms of a rescaled dimensionless interception efficiency η/Da in Figure 13. This figure shows the variation of η/Da with L_r and compares it with the analytical expressions derived in the limits of high and low blockage ratio. In the limit of high blockage ratio ($L_r < 2$), the numerical data and equation (22) are in good agreement. In the limit of low blockage ratio (large L_r), the additional viscous resistance of the side channels between the cylinder and the walls is negligible and the numerical data converge to the expression given by equation (34). Furthermore, Figure 13 shows that in the limit of large relative plate separation ($L_r > 50$), $\eta/Da \lesssim 10$. Hence, for most practical Darcy numbers ($Da < 10^{-3}$), the interception efficiency of a porous cylinder in an unbounded flow is very low ($\eta < 0.01$). The bounding presence of a wall strongly enhances the interception efficiency, especially when the walls are close to the cylinder ($L_r < 2$). Clearly, the design trade-off that must be made during device optimization is between the pressure drop and the interception efficiency since both increase as L_r approaches unity.

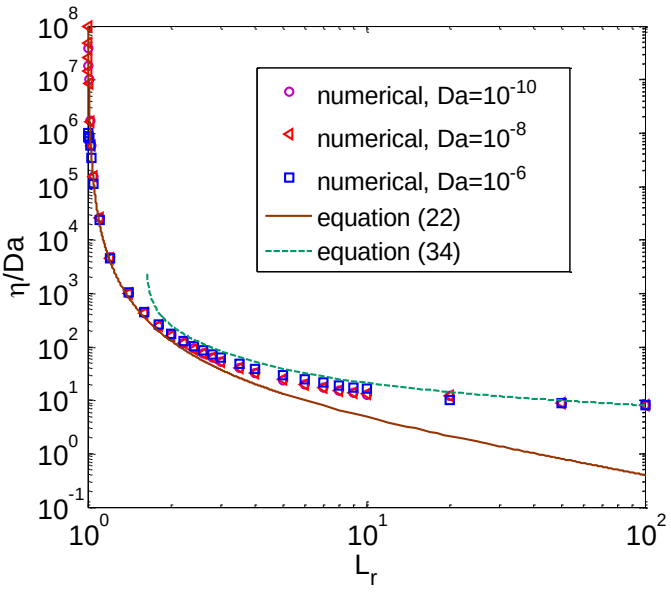

Figure 13: Scaled interception efficiency η/Da varying with plates spacing ratio L_r at $Da = 10^{-10}$, 10^{-8}, 10^{-6} and $Re_D = 1$: comparison of numerical data (symbols) with analytical limits for $L_r \to 1$, equation (22), and $L_r \to \infty$, equation (34).

In the analytical expressions derived for the flow interception efficiency, the pressure resistance of the porous cylinder was approximated using a resistance network model by assuming that the cylinder consists of a series of infinitesimally thin parallel elements. This method yielded good agreement with full numerical simulations and can also be used for estimating the pressure resistance and drag coefficient of other porous bodies of known surface profile when the Reynolds number based on pore size is less than unity.

The analyses presented in this study have focused exclusively on Newtonian fluids. In applications involving complex fluids such as polymer solutions, microgels, or suspensions, the non-Newtonian characteristics can significantly affect the flow behavior. We believe it is possible to extend the approach presented in this study to the flow of generalized Newtonian fluids using a modified version of Darcy's law that accounts for the shear-rate–dependent viscosity.

Although in our analysis we have considered a single confined porous cylinder, we expect to see similar trends when the confinement is due to the presence of other low permeability features rather than just parallel impermeable plates. For instance, in the case of a periodic array of porous cylinders, equation (22) is still valid, except we will

require a modified form of the geometric function $I(L_r)$, which can be obtained from solving the velocity-pressure relationship for flow through the gap between two parallel cylinders. In such a case, the geometric parameter L_r would become the ratio of the cylinders spacing to diameter, $L_r = S/D$, where S is the center-to-center distance of the two adjacent cylinders. A biomicrofluidic sensor system consisting of an array of porous cylinders composed of vertically aligned carbon nanotubes has recently been assembled for bioparticle isolation (Chen et al., 2012) .

We note that in the present work we have computed the convective flow efficiency (or "flow interception efficiency") that arises from the systematic changes in the kinematics of the flow as the cylinder permeability, flow geometry and fluid inertia are changed. In calculating an overall particle interception efficiency for use in bioparticle capture and isolation applications, there are additional mechanisms beyond the flow kinematics that also contribute to particle interception efficiency, such as diffusion, inertial impaction, and gravitational sedimentation (Spielman, 1977). Each of these mechanisms gives an additional contribution to the overall particle interception efficiency and introduces an additional dimensionless parameter (such as the Péclet number and Stokes number of the suspended particles in the fluid or the reaction Damköhler number in the case of chemical binding of particles to the porous cylinder). Numerical evaluation of the flow efficiency values using the formulae developed in the present study and comparison with the efficiencies obtained from these other mechanisms can help optimize the kinematic design of biomicrofluidic devices based on porous sensing elements to ensure maximum particle collection efficiency.

Acknowledgment

The authors thank Prof. Michael F. Rubner (MIT DMSE), Prof. Mehmet Toner (MIT HST & Harvard-MGH), and Allison Yost (MIT MechE) for their valuable comments. This work was supported in part by the MRSEC Program of the National Science Foundation under award number DMR-0819762. SS thanks the Mechanical Engineering Department at MIT for the Rohsenow Fellowship.

References

Babu, V., Narasimhan, A., 2010. Investigation of vortex shedding behind a porous square cylinder using lattice Boltzmann method. Physics of Fluids 22, 053605.

Bhattacharyya, S., Dhinakaran, S., Khalili, A., 2006. Fluid motion around and through a porous cylinder. Chemical Engineering Science 61, 4451-4461.

Bhattacharyya, S., Singh, A.K., 2011. Reduction in drag and vortex shedding frequency through porous sheath around a circular cylinder. International Journal for Numerical Methods in Fluids 65, 683-698.

Chen, G.D., Fachin, F., Colombini, E., Wardle, B.L., Toner, M., 2012. Nanoporous micro-element arrays for particle interception in microfluidic cell separation. Lab on a Chip 12, 3159-3167.

Chen, J.H., Pritchard, W.G., Tavener, S.J., 1995. Bifurcation for flow past a cylinder between parallel planes. Journal of Fluid Mechanics 284, 23-41.

Chen, X., Cui, D.-F., Liu, C.-C., Li, H., 2007. Microfabrication and characterization of porous channels for DNA purification. Journal of Micromechanics and Microengineering 17, 68.

Drott, J., Rosengren, L., Lindström, K., Laurell, T., 1999. Porous silicon carrier matrices in micro enzyme reactors-influence of matrix depth. Microchimica Acta 131, 115-120.

Ergun, S., 1952. Fluid flow through packed columns. Chemical Engineering Progress 48, 89-94.

Fachin, F., Chen, G.D., Toner, M., Wardle, B.L., 2011. Integration of Bulk Nanoporous Elements in Microfluidic Devices With Application to Biomedical Diagnostics. Microelectromechanical Systems, Journal of 20, 1428-1438.

Faxén, O.H., 1946. Forces exerted on a rigid cylinder in a viscous fluid between two parallel fixed planes. Generalstabens litografiska anstalts förlag.

Happel, J., Brenner, H., 1983. Low Reynolds Number Hydrodynamics: With Special Applications to Particulate Media. M. Nijhoff.

James, D.F., Davis, A.M., 2001. Flow at the interface of a model fibrous porous medium. Journal of Fluid Mechanics 426, 47-72.

Jue, T.-C., 2004. Numerical analysis of vortex shedding behind a porous square cylinder. International Journal of Numerical Methods for Heat & Fluid Flow 14, 649-663.

Liu, Z.G., Wang, P.K., 1997. Pressure drop and interception efficiency of multifiber filters. Aerosol science and technology 26, 313-325.

Neale, G., Epstein, N., Nader, W., 1973. Creeping flow relative to permeable spheres. Chemical Engineering Science 28, 1865-1874.

Sahin, M., Owens, R.G., 2004. A numerical investigation of wall effects up to high blockage ratios on two-dimensional flow past a confined circular cylinder. Physics of Fluids 16, 1305-1320.

Shi, Y.-Y., Braden Jr, R., 1966. The effect of permeability on low Reynolds number flow past a circular porous cylinder. Develop. Theoret. Appl. Mech 3, 761-775.

Singh, M.P., Gupta, J.L., 1971. The flow of a viscous fluid past an inhomogeneous porous cylinder. ZAMM - Journal of Applied Mathematics and Mechanics / Zeitschrift für Angewandte Mathematik und Mechanik 51, 17-25.

Singha, S., Sinhamahapatra, K.P., 2010. Flow past a circular cylinder between parallel walls at low Reynolds numbers. Ocean Engineering 37, 757-769.

Spielman, L., 1977. Particle Capture from Low-Speed Laminar Flows. Annual Review of Fluid Mechanics 9, 297-319.
Sutherland, D.N., Tan, C.T., 1970. Sedimentation of a porous sphere. Chemical Engineering Science 25, 1948-1950.
Tamayol, A., Bahrami, M., 2011. Transverse permeability of fibrous porous media. Physical Review E 83, 046314.
Tufenkji, N., Elimelech, M., 2004. Correlation equation for predicting single-collector efficiency in physicochemical filtration in saturated porous media. Environmental Science & Technology 38, 529-536.
Vafai, K., 1984. Convective flow and heat transfer in variable-porosity media. Journal of Fluid Mechanics 147, 233-259.
Vanni, M., 2000. Creeping flow over spherical permeable aggregates. Chemical Engineering Science 55, 685-698.
Whitaker, S., 1996. The Forchheimer equation: A theoretical development. Transport in Porous Media 25, 27-61.
White, F.M., 2011. Fluid Mechanics. McGraw-Hill Higher Education.
Yu, P., Zeng, Y., Lee, T.S., Chen, X.B., Low, H.T., 2011. Steady flow around and through a permeable circular cylinder. Computers & Fluids 42, 1-12.
Zovatto, L., Pedrizzetti, G., 2001. Flow about a circular cylinder between parallel walls. Journal of Fluid Mechanics 440, 1-25.